Investigation of a polar form of fluoroethylene dimer, $(C_2H_3F)_2$, by microwave spectroscopy

Melissa A. Martinez,[a] Channing T. West,[b] Brooks H. Pate,[b] Sean A. Peebles,[a] Rebecca A. Peebles[a] *

[a] Department of Chemistry and Biochemistry, Eastern Illinois University, 600 Lincoln Avenue, Charleston, IL 61920, USA

[b] Department of Chemistry and Biochemistry, University of Virginia, McCormick Rd., PO Box 400319, Charlottesville, VA 22904, USA

*To whom correspondence should be addressed:
Email: rpeebles@eiu.edu
Phone: 1(217) 581-3322

Abstract

The structure of fluoroethylene dimer ($(C_2H_3F)_2$, $(FE)_2$) has been determined using chirped-pulse Fourier-transform microwave (CP-FTMW) spectroscopy. Although the most stable structure was expected to be nonpolar, a planar, polar configuration was observed with sufficient intensity to measure spectra for four unique ^{13}C substituted isotopologues in natural abundance. This allowed a least-squares fit of the structural parameters of the dimer to observed moments of inertia. The resulting structure has a T-shaped arrangement of C=C bonds, similar to the recently studied FE···1,1-difluoroethylene complex. Both dimers contain a cyclic arrangement of CH···F contacts between the H-C-F end of one monomer and the H-C=C-F side of the second monomer. ωB97X-D/6-31+G(d,p), MP2/6-311++G(2d,2p) and MP2/aug-cc-pVDZ calculations give the expected nonpolar end-to-end structure, ranging from 9 cm^{-1} (DFT) to 63 cm^{-1} and 57 cm^{-1} (MP2/6-311++G(2d,2p) and aug-cc-pVDZ, respectively) more stable than the experimentally observed orientation. The ωB97X-D/6-31+G(d,p) calculations also indicate a nonplanar, polar configuration that is over 60 cm^{-1} more favorable than the nonpolar structure; however, MP2 calculations predict significantly higher energy, and spectroscopic results provide no evidence of that structure's existence. The rotational constants of the observed T-shaped $(FE)_2$ structure are A = 6582.8323(12) MHz, B = 1256.6203(4) MHz, C = 1060.3474(3) MHz, and the dipole moment components, determined *via* Stark effect measurements, are μ_a = 0.683(3) D, μ_b = 0.301(5) D, μ_{tot} = 0.746(5) D.

Keywords: weak hydrogen bond; chirped-pulse; rotational spectroscopy; Stark effect; vinyl fluoride; fluoroethene

I. Introduction

As part of a larger project to study different sized clusters of fluoroethylene (FE) with CO_2, a chirped-pulse Fourier-transform microwave spectroscopy (CP-FTMW) scan of fluoroethylene was performed in order to eliminate transitions that required only FE from consideration for FE/CO_2 studies. The rotational spectrum of FE monomer itself [1] is very sparse in the 2-8 GHz range of the present study; however, the scan covering this frequency range was quite dense (Figure 1), averaging over 1 line per 2 MHz of spectrum (with signal to noise ratio (S/N) above 3). It is clear that spectra of many different weakly bound clusters involving FE must be present within this data set. This presence of spectra for many species raises an increasingly common question in broadband rotational spectroscopy: should researchers focus on identifying spectra of specific species of interest to them and ignore remaining unassigned transitions, or should the aim be to assign and identify carriers of all visible spectra within a given scan? Identification of the components of complex mixtures is an important challenge for potential industrial applications of microwave spectroscopy [2, 3, 4], and identification of spectra of the many clusters present within a single supersonic expansion provides a venue to develop and test analytical approaches that could later be applied in such applications. In the present work, identification of the species present in an expansion of FE in neon will allow further testing of techniques being developed and implemented in related studies of FE/CO_2 and 1,1-difluoroethylene (1,1-DFE)/CO_2 clusters [5, 6]. Possible species present in a scan of FE-only include $(FE)_2$, $(FE)_3$ and larger FE clusters, as well as FE···H_2O, and complexes of FE with the carrier gas (in this case Ne). None of these species have been previously reported in the literature, although FE···Ne is presently under analysis in our lab, and we believe we have

also identified spectra for $(FE)_3$ and $(FE)_4$. Neon-containing and larger FE clusters will be discussed in future publications [5, 7, 8].

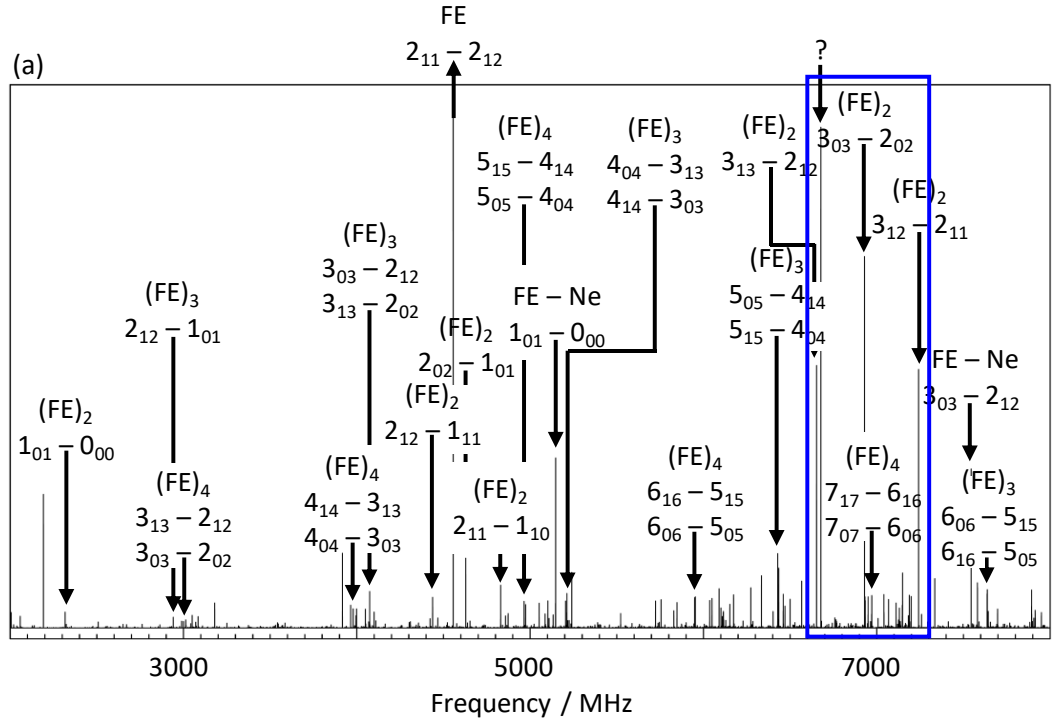

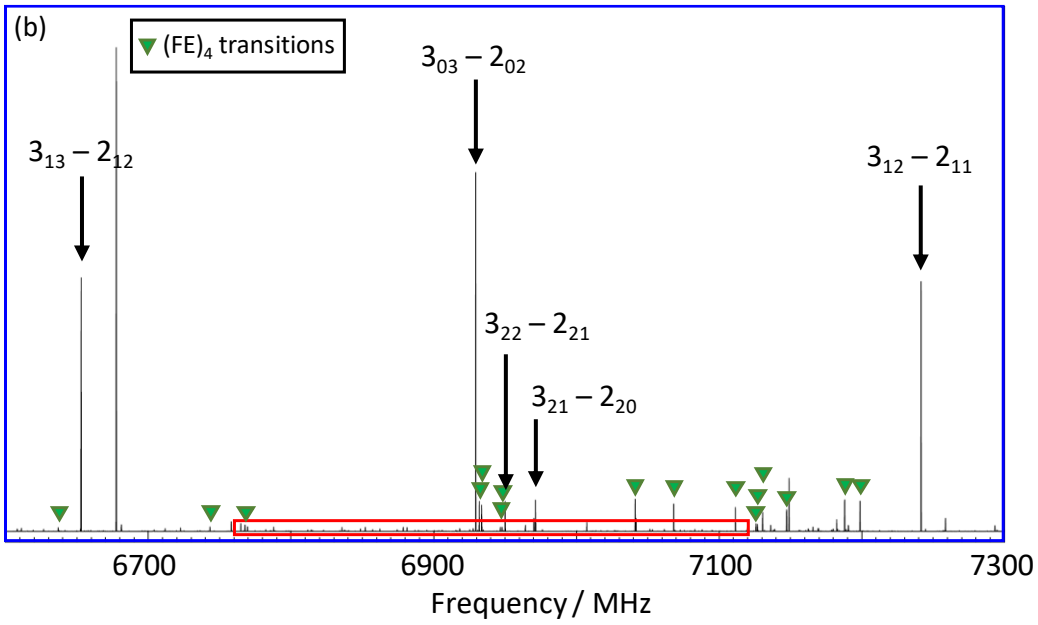

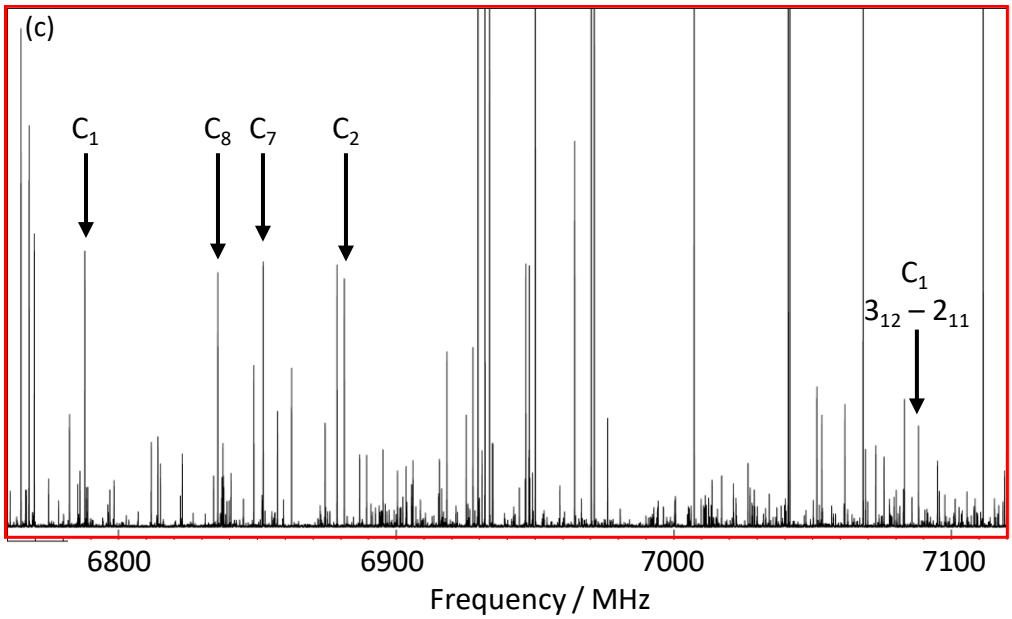

Figure 1. Microwave spectrum of fluoroethylene in neon. See text for experimental details. (a) Full 2 – 8 GHz spectrum, with vertical scale magnified approximately ×2, with the strongest assigned transitions labeled. Although spectra labeled $(FE)_3$ and $(FE)_4$ have been fitted to constants consistent with these species, cluster composition is unconfirmed [8]. (b) Magnification of the 6.6 - 7.3 GHz range (blue box in figure (a)), with vertical axis unchanged, showing $J = 2 \leftarrow 3$ transitions of $(FE)_2$. Transitions labeled with triangles are assigned to the species that is believed to be $(FE)_4$. (c) Magnification of the 6760 – 7120 MHz range (red box in figure (b)), showing transitions from ^{13}C-containing isotopologues in natural abundance, with atom numbers as shown in Figure 2.

FE dimers and larger clusters are likely to have structures dominated by weak CH···F and/or CH···π interactions. We previously determined the structure of the FE···1,1-DFE dimer, and found a planar T-shaped orientation of the double bonds, with the C=C bond of 1,1-DFE forming the top of the T and the C=C bond of FE forming the post of the T [9] (Figure 2(b)). This structure includes a cyclic arrangement of CH···F contacts, with the molecules both containing a fluorine atom acting as CH···F acceptor and a hydrogen atom acting as CH···F donor. The lower symmetry of FE compared to 1,1-DFE, and the combination of two identical monomer building blocks, makes a nonpolar $(FE)_2$ dimer seem likely; however, it is possible that a polar T-shaped dimer similar to FE···1,1-DFE could also exist. If T-shaped $(FE)_2$ can be

identified and its structure determined, then this will provide an ideal opportunity to probe changes in the strength and orientation of weak CH···F interactions between the singly and doubly fluorinated species. In the following sections, we present both theoretical and microwave spectroscopic results on the polar $(FE)_2$ complex, including a full experimental structure determination.

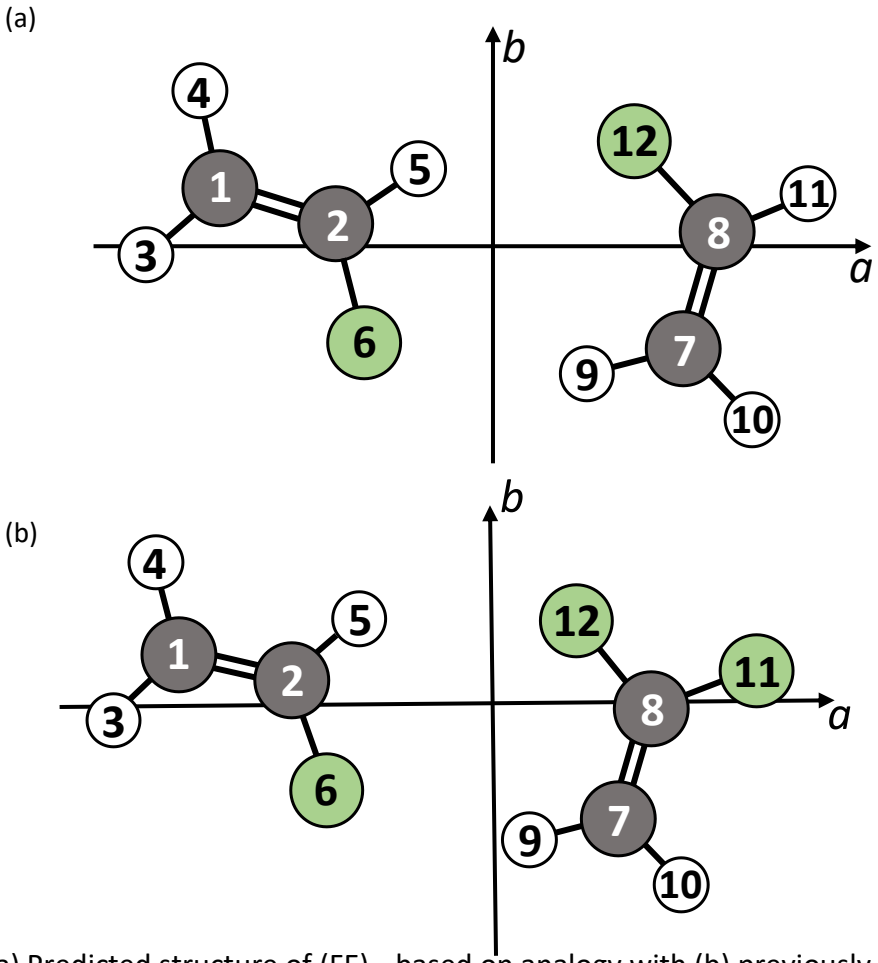

Figure 2. (a) Predicted structure of $(FE)_2$, based on analogy with (b) previously published work on FE··· 1,1-DFE [9]. Atom numbers are utilized for structural comparisons (see text).

II. Experimental Methods

A scan of 1 million free induction decays (FIDs) was recorded with a mixture of 1% fluoroethylene (98%, Synquest Labs) in neon carrier gas (Praxair) using the 2 – 8 GHz chirped-

pulse Fourier-transform microwave spectrometer (CP-FTMW) at the University of Virginia (UVa) [2,10]. The sample was delivered through five nozzles (1 mm diameter) to the spectrometer at a backing pressure of 2 atm, with 24 FIDs recorded per nozzle pulse. The nozzle repetition rate was 3 Hz. Kisiel's AABS suite [11] was used to facilitate spectral analysis, with Pickett's CALPGM (SPFIT and SPCAT) package used for spectroscopic fitting and prediction [12]. Stark effect measurements for dipole moment determination were made using the Balle-Flygare FTMW spectrometer at Eastern Illinois University (EIU) [13, 14]. Voltages of up to ±5 kV were applied across two steel mesh plates spaced about 31 cm apart above and below the Fabry-Perot cavity of the spectrometer, and electric field calibration was performed assuming an OCS dipole of 0.71519(3) D [15].

Ab initio calculations utilized Gaussian 09 and were performed at ωB97X-D/6-31+G(d), MP2/6-311++G(2d,2p) and MP2/aug-cc-pVDZ levels, using G09W for DFT calculations and G09 on a Linux workstation for MP2 calculations [16, 17]. Vibrational frequency calculations at the MP2 level (with tight convergence criteria for both SCF energy and structure optimizations) were used to determine whether observed stationary points were true minima on the potential energy surface of the dimer, and also allowed calculation of zero-point energy (ZPE) corrections for optimized dimer structures.

III. Results and Discussion

A. Spectra

According to preliminary MP2 calculations on $(FE)_2$ performed at the time of an earlier study of FE···CO_2 dimers [18], the lowest energy structures were expected to be nonpolar, with relative energies of the most stable polar structures being too high to have significant population

in the molecular expansion; however, when a 1 million FID spectrum of FE was recorded as part of more recent studies of larger FE/CO_2 clusters [6], spectra of several unidentified species requiring only FE were assigned [5, 8]. The intensities and rotational constants of these were consistent with trimers or larger clusters, and a considerable number of stronger unassigned lines, at intensities closer to those expected for dimers, remained in the spectrum (Figure 1(a)). This prompted us to revisit the possibility of observing the rotational spectrum for a polar $(FE)_2$ configuration. After elimination of a few FE monomer transitions, over 1000 lines with signal-to-noise (S/N) greater than 10 remained in the spectrum. Emphasis was put on assigning these lines to previously unknown species. FE···Ne and FE···H_2O spectra were predicted to be sparse in the available 2 – 8 GHz frequency range; thus, our focus was on a polar form of $(FE)_2$. A prediction assuming a structure similar to FE···1,1-DFE [9] (see Section III.B.) gave a strong *a*-type pattern, and comparison with the experimental spectrum immediately suggested an assignment of several of the strongest observed lines to $K_a = 0$ and 1 transitions for $J'' = 2$ (Figure 1(a, b)). The spectrum was fitted to a Watson *A*-reduction Hamiltonian in the I^r representation, with a total of 21 *a*- and *b*-type transitions fitted to six constants with an RMS deviation of 3.2 kHz. There are only two transitions with $K_a = 2$ in the fit, and these have (observed – calculated) frequency deviations of 5 to 10 kHz, which is larger than the expected experimental reproducibility of ~4 kHz. Addition of another fourth order distortion constant, δ_K, to the Hamiltonian, allows these transitions to fit much better, with deviations of less than 3 kHz; however, the δ_K constant is strongly correlated with *B* and *C* and causes additional correlations between the other constants. Finally, a Watson *S*-reduction fit was performed, with the *S*-reduction constant d_2 replacing δ_K. This led to a more satisfactory fit, with constants and an overall *RMS* that are not significantly different than the *A*-reduction that included δ_K, but without

the correlation problems. The *S*-reduction is our preferred result. Constants resulting from both the original *A*-reduction and the final *S*-reduction fits are given in Table 1 for comparison. Fitted constants give an asymmetry parameter, κ, of -0.9289, consistent with a near-prolate asymmetric top and the use of an *S*-reduction Hamiltonian.

Table 1. Fitted spectroscopic constants for $(FE)_2$, showing both *S*-reduction (preferred) and *A*-reduction fits, and results for all four singly substituted ^{13}C isotopologues (see Figure 2(a) for atom numbers).[a]

	"Normal"	"Normal" – *A*-Reduction	$^{13}C_1$	$^{13}C_2$	$^{13}C_7$	$^{13}C_8$
A / MHz	6582.8323(12)	6582.834(2)	6551.3(7)	6577.3(10)	6477.7(14)	6579.8(2)
B / MHz	1256.6203(4)	1256.6190(5)	1229.2402(5)	1247.2025(9)	1243.1467(10)	1238.17936(19)
C / MHz	1060.3474(3)	1060.3482(4)	1040.0216(5)	1053.5221(9)	1048.0575(10)	1047.15292(19)
D_J / kHz	1.609(10)	1.591(15)[e]	[1.609]	[1.609]	[1.609]	[1.609]
D_{JK} / kHz	26.82(5)	26.81(9)[e]	24.40(14)	26.6(2)	25.4(3)	26.30(5)
d_1 / kHz	-0.190(3)	0.172(2)[e]	[-0.190]	[-0.190]	[-0.190]	[-0.190]
d_2 / kHz	-0.075(13)		[-0.075]	[-0.075]	[-0.075]	[-0.075]
P_{aa} / u Å^2 [b]	401.00867(13)	401.0087(2)	409.961(4)	404.039(6)	405.360(9)	406.9887 (15)
P_{bb} / u Å^2 [b]	75.60776(13)	75.6074(2)	75.971(4)	75.666(6)	76.846(9)	75.6333(15)
P_{cc} / u Å^2 [b]	1.16452(13)	1.1649(2)	1.171(4)	1.171(6)	1.172 (9)	1.1743(15)
N[c]	21	21	8	9	8	8
RMS / kHz[d]	3.2	3.2	1.6	2.9	2.9	0.6

[a] Errors in parentheses correspond to one standard deviation.
[b] P_{aa}, P_{bb} and P_{cc} are planar moments, $P_{xx} = 0.5(P_{yy} + P_{zz} - P_{xx})$, for permutations of $(a, b, c) = (x, y, z)$.
[c] *N* = number of transitions in the fit.
[d] *RMS* = root-mean-square deviation of (observed – calculated) frequencies for fitted transitions (listed in Table 2). $RMS = \left(\frac{(\Sigma(\nu_{obs}-\nu_{calc})^2)}{N}\right)^{1/2}$.
[e] *A*-reduction distortion constants are Δ_J, Δ_{JK} and δ_J.

Transitions for the dimer were sufficiently intense that it was possible to assign spectra for the four unique ^{13}C isotopologues in natural abundance within the broadband scan. The strongest ^{13}C transitions have S/N in excess of ~20 (Figure 1(c)). For each of these spectra, a

total of 8 or 9 transitions were assigned, while keeping all distortion constants except D_{JK} fixed to values from the normal species. This gave *RMS* deviations for ^{13}C fits of 0.5-3 kHz. Fitted constants are listed in Table 1, and transition frequencies are given in Table 2. Searches for transitions consistent with other predicted structures (Section III.B.) were unsuccessful.

B. *Ab Initio* Calculations

Initial optimizations of $(FE)_2$ were performed using density functional theory (DFT) at the ωB97X-D/6-31+G(d,p) level. This quickly provided a series of dimer structural predictions, that could be benchmarked against MP2/6-311++G(2d,2p) calculations, which have previously been applied to many similar systems (for example [6, 9, 18, 19]). As described below, we later also performed the same set of calculations at the MP2/aug-cc-pVDZ level. In addition to needing a thorough investigation of likely $(FE)_2$ structures to guide the spectroscopic investigations, comparison with MP2 results is important as we search for a faster alternative to the MP2 studies, which will rapidly become unfeasible as cluster size increases. For the present system, optimizations at both DFT and MP2 levels were hindered by very flat potential energy surfaces, which allowed relatively large structural changes to occur with minimal variation in energy. Although not applied directly to the present $(FE)_2$ study, ongoing investigations of $(FE)_n$ and $(FE)_n(CO_2)_m$ clusters are utilizing an artificial intelligence algorithm based on bee colonies, *via* ABCluster code [20, 21], to provide predictions of the most likely structural arrangements. This allows the most likely structural arrangements to be rapidly selected for further study using more expensive DFT or MP2 methods.

Table 2. Assigned transitions for $(FE)_2$, for the normal and all four ^{13}C isotopologues. For the normal species, observed-calculated deviations are presented for both the preferred *S*-reduction fit and for the *A*-reduction fit (see Table 1 and text for details).

						Obs-Calc [a]		$^{13}C_1$		$^{13}C_2$		$^{13}C_7$		$^{13}C_8$	
J′	K_a'	K_c'	*J″*	K_a''	K_c''	Frequency / MHz	*S*-Reduction (preferred)	*A*-Reduction	Frequency / MHz	Obs-Calc [a]	Frequency / MHz	Obs-Calc [a]	Frequency / MHz	Obs-Calc [a]	Frequency / MHz	Obs-Calc [a]
1	0	1	0	0	0	2316.9629	1.5	2.0			2300.7214	3.3	2291.2043	6.5		
6	1	5	6	1	6	4113.5096	-4.4	-4.2								
4	0	4	3	1	3	4355.8975	0.5	3.0								
2	1	2	1	1	1	4437.5095	-0.4	-1.3	4349.1610	-0.8	4407.6197	2.9	4387.1727	0.6	4379.4879	0.3
2	0	2	1	0	1	4628.5598	0.7	1.2	4533.5146	-1.2	4596.2125	-2.2	4577.0029	-2.0	4565.5793	-1.4
2	1	1	1	1	0	4830.0458	2.2	4.1	4727.5839	-3.1	4794.9709	5.5	4777.3407	2.3	4761.5284	0.1
7	1	6	7	1	7	5475.6276	3.7	0.2								
1	1	0	1	0	1	5522.4285	-2.0	-2.8								
2	1	1	2	0	2	5723.9149	-0.1	0.5								
3	1	2	3	0	3	6036.0414	-0.8	1.2								
4	1	3	4	0	4	6470.4126	-0.2	2.1								
3	1	3	2	1	2	6652.8949	-0.5	-2.1	6520.5999	0.3	6608.1421	-0.7	6577.3710	-1.7	6566.0417	0.3
3	0	3	2	0	2	6929.4555	-0.4	-0.9	6787.8111	1.1	6881.2922	-1.4	6852.0596	1.2	6835.7175	0.0
3	2	2	2	2	1	6950.0923	-0.7	5.8	6807.0320	-1.1	6901.3697	1.9	6872.8365	0.6	6855.1990	-0.1
5	0	5	4	1	4	6970.2448	0.4	-0.4								
3	2	1	2	2	0	6971.3494	-2.8	-10.3	6826.8214	1.2	6922.0572	-2.5			6875.2901	-0.2
8	1	7	8	1	8	7022.5722	-1.3	0.8								

5	1	4	5	0	5	7041.8001	0.2	1.3							
3	1	2	2	1	1	7241.5835	0.3	1.2	7088.1353	1.8	7189.0542	-2.4	7162.5048	-2.9	7138.9974	0.5
1	1	1	0	0	0	7643.1219	1.5	-0.6							
6	1	5	6	0	6	7767.1411	2.6	0.9							

[a] Observed – Calculated frequency, in kHz, based on fitted constants reported in Table 1.

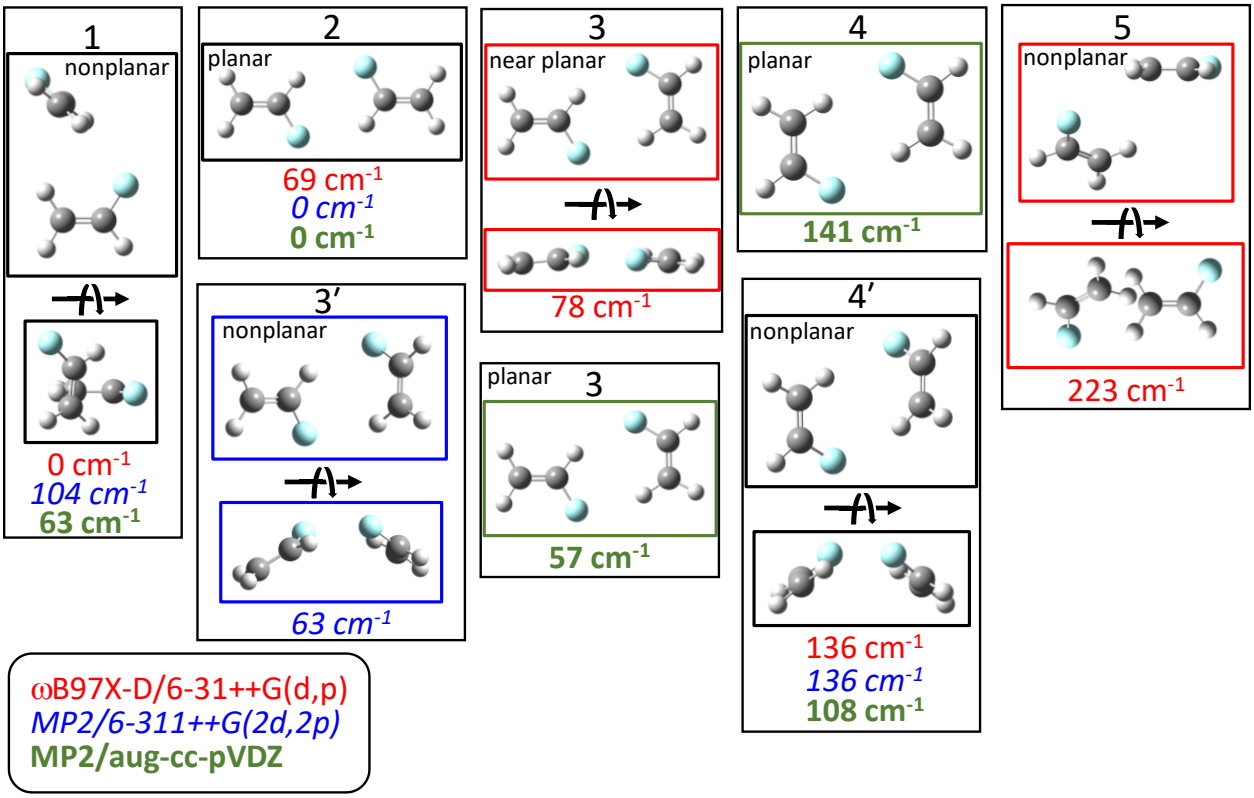

Figure 3. Optimized structures for $(FE)_2$. Relative energies are given below each structure, with the top (red) value corresponding to the ωB97X-D/6-31+G(d,p) optimization, and the middle (blue italic) and bottom (green bold) values corresponding to zero-point-energy corrected MP2/6-311++G(2d,2p) and MP2/aug-cc-pVDZ calculations, respectively. In most cases, results of the three calculations are visually similar enough that only one structure is shown. See text and Tables 3 and 4 for further details. For Structure 2, C_{2h} symmetry was enforced for the MP2 calculations, while symmetry was not enforced for the DFT calculation.

Table 3. Rotational constants, dipole moment components, and relative energies of optimized structures for $(FE)_2$, at DFT level (ωB97X-D/6-31+G(d,p)). See Figure 3 for structure illustrations.

Structure Number:	1	2	3	4′	5
ΔE / cm^{-1}	0	69	78	136	223
A / MHz	5916.0	9624.8	6316.4	5196.5	7128.3
B / MHz	1211.7	1092.2	1270.7	1417.7	984.0
C / MHz	1153.5	980.9	1060.2	1220.4	887.1
P_{aa} / u $Å^2$	384.9	462.7	397.2	336.7	506.2
P_{bb} / u $Å^2$	53.2	52.5	79.5	77.4	63.5
P_{cc} / u $Å^2$	32.2	0.0	0.5	19.8	7.4
μ_a / D	2.3	0.0	0.9	0.0	1.4
μ_b / D	0.5	0.0	0.3	0.0	0.4
μ_c / D	0.6	0.0	0.2	1.9	0.3
μ_{tot} / D	2.4	0.0	1.0	1.9	1.5

Table 4. Rotational constants, dipole moment components, and relative energies of optimized structures for $(FE)_2$, at MP2/6-311++G(2d,2p) and MP2/aug-cc-pVDZ levels. See Figure 3 for structure illustrations. See text for discussion of effects of basis set choice on results.

Structure Number:	1	2	3	3′	4	4′
MP2/6-311++G(2d,2p)						
ΔE / cm^{-1}	84	0	68	58	165	119
ΔE ZPE / cm^{-1} [a]	104	0	--	63	--	136
A / MHz	5999.4	10428.0	6404.8	5701.5	5282.3	5199.0
B / MHz	1218.3	1107.3	1278.9	1349.7	1367.5	1438.1
C / MHz	1165.5	1001.0	1066.0	1196.2	1086.3	1230.7
P_{aa} / u Å^2	382.1	456.4	395.2	354.1	369.6	332.4
P_{bb} / u Å^2	51.5	48.5	78.9	68.3	95.7	78.2
P_{cc} / u Å^2	32.7	0.0	0.0	20.3	0.0	19.0
μ_a / D	2.3	0.0	0.8	0.7	0.0	0.0
μ_b / D	0.5	0.0	0.3	0.3	0.0	0.0
μ_c / D	0.5	0.0	0.0	1.4	0.0	1.7
μ_{tot} / D	2.5	0.0	0.9	1.7	0.0	1.7
MP2/aug-cc-pVDZ						
ΔE / cm^{-1}	71	0	23	--	127	118
ΔE ZPE / cm^{-1} [a]	63	0	57	--	141	108
A / MHz	5811.7	9223.1	6088.5	--	5174.4	5086.8
B / MHz	1228.2	1118.8	1296.3	--	1386.0	1456.5
C / MHz	1177.8	997.7	1068.8	--	1093.2	1251.0
P_{aa} / u Å^2	376.8	451.7	389.9	--	364.6	325.8
P_{bb} / u Å^2	52.3	54.8	83.0	--	97.7	78.2
P_{cc} / u Å^2	34.7	0.0	0.0	--	0.0	21.2
μ_a / D	2.3	0.0	0.8	--	0.0	0
μ_b / D	0.5	0.0	0.3	--	0.0	0
μ_c / D	0.6	0.0	0.0	--	0.0	1.7
μ_{tot} / D	2.4	0.0	0.9	--	0.0	1.7

[a] Zero-point-energy corrected relative energies.

DFT calculations gave five unique structures (Figure 3, Tables 3 and 4). With the relatively small basis set employed (6-31+G(d,p)), a nonplanar arrangement with the F atom of one FE pointing towards the H-C=C-H side of the second FE (Structure 1) is about 69 cm^{-1} lower in energy than the most stable planar structure. In the most favorable planar structure, the H-C-F ends of the FE molecules point towards each other, forming a cyclic arrangement of two CH···F interactions (Structure 2). A similar expected planar arrangement, with interactions between the two H-C=C-F sides of the FE molecules, converges to a non-planar book-like structure (Structure 4′), which is fourth lowest energy overall (136 cm^{-1} above the minimum). The only other (near) planar arrangement involves a T-shaped orientation of the C=C bonds (Structure 3), with the end H-C-F of one FE molecule pointing towards the side H-C=C-F of the second FE, in a structure very similar to that observed for 1,1-DFE···FE [9]. This arrangement is predicted, at DFT level, to be 78 cm^{-1} higher in energy than the most stable configuration. The final $(FE)_2$ configuration obtained at ωB97X-D/6-31+G(d,p) level lies significantly higher in energy (223 cm^{-1} above the minimum) and appears to involve both CH···π and CH···F contacts between the two monomers (Structure 5).

Calculations at the MP2/6-311++G(2d,2p) level led to a total of four stationary points (Figure 3, Table 4), and vibrational frequency calculations revealed that all four are true minima on the potential energy surface. Zero-point energy (ZPE) corrected relative energies are not significantly different from uncorrected values (Table 4). At MP2 level (and with a larger basis set, compared to the DFT calculations), the minimum energy configuration is the nonpolar planar end-to-end arrangement that was second most stable at DFT level (Structure 2). The book-like structure (Structure 4′) remains fourth lowest, lying 136 cm^{-1} above Structure 2 after ZPE corrections. The nonplanar Structure 1, which was most stable at DFT level, is now third lowest

(104 cm^{-1} above the minimum), while T-shaped Structure 3 now converges to a nonplanar (book-like) arrangement (3′) lying 63 cm^{-1} above the minimum after ZPE corrections. Extensive efforts at optimizing additional structures only led to a planar version of this arrangement if symmetry was enforced during the optimization.

During review of this manuscript we became aware that Pople basis sets such as 6-311++G(2d,2p) have known limitations in optimization of planar structures [22]; thus, we performed an additional set of MP2 calculations using the aug-cc-pVDZ basis set, which has the same number of basis functions as 6-311++G(2d,2p). These results are also included in Table 4. The T-shaped Structure 3 now only resulted in a planar optimized structure, even when the optimization was begun from the nonplanar 3′ configuration. For Structure 4, both planar and nonplanar optimized arrangements were obtained. Frequency calculations at the MP2/aug-cc-pVDZ level gave only real frequencies for all converged structures, although the lowest frequency vibrations for both Structures 3 and 4 correspond to out-of-plane distortions towards the book-like 3′ and 4′ configurations. ZPE corrected energy differences are similar to 6-311++G(2d,2p) values, with aug-cc-pVDZ results predicting Structure 3 to lie 57 cm^{-1} above minimum energy Structure 2. Planar, nonpolar Structure 4 is now 141 cm^{-1} above the minimum, while the book-like 4′ appears still to be slightly more stable, at 108 cm^{-1} above the minimum. Structure 1 is now only 6 cm^{-1} less stable than Structure 3 (63 cm^{-1} above the minimum). Structure 5, which was 223 cm^{-1} above the minimum at DFT level, was not obtained as a stationary point at MP2/6-311++G(2d,2p) level, and was not optimized with the aug-cc-pVDZ basis set.

Spectroscopic predictions were made based on the two lowest energy polar structures from the DFT calculations (Structures 1 and 3), and patterns very similar to those predicted for

Structure 3 were quickly identified in the broadband microwave scan (see Section III.A., above). Particularly because of the differences in energy ordering between the DFT and MP2/6-311++G(2d,2p) calculations, as well as uncertainty about the degree of planarity (with potential large effects on rotational constants and dipole moment components), searches were also carried out for Structure 4′ based on MP2 predictions. Although some reasonably strong unassigned transitions remain in the spectrum, no additional dimer configurations have yet been identified.

In general, it was found that rotational constants and relative magnitudes of dipole moment components were in very good agreement between the ωB97X-D/6-31+G(d,p) and both sets of MP2 calculations; however, the energy ordering of observed dimer configurations was very different between the DFT and MP2 theoretical approaches. Experimental evidence from this and a recent study of 1,1-DFE···FE [9], indicates that the MP2 ordering is likely more accurate than the DFT results. The lack of planarity observed for MP2/6-311++G(2d,2p) Structures 3′ and 4′ was originally disconcerting; however, the MP2/aug-cc-pVDZ calculations prompted by Reference 22 now suggest that planar configurations are likely, and these results are consistent with experimental observations, both here and in Reference 9. Spectroscopically, the much faster DFT methods utilized in the present work give reliable enough estimates of rotational constants to facilitate identification of species present in the spectrum. They would suffice for initial spectroscopic searches and assignments (although the questions about planarity require that predicted dipole components be interpreted very loosely). Higher level calculations would be necessary for reliable comparison of structural details, energetics, and electronic properties, with use of non-Pople basis sets helping to ensure that difficulties with optimization of planar stationary configurations are avoided.

C. Structure

Initial comparison of fitted rotational constants with theoretical predictions led to a clear preference for planar Structure 3. The planar moment, P_{cc}, from the assigned spectrum is 1.16452(13) u Å^2, confirming a planar arrangement of FE molecules (where $P_{xx} = \sum_i m_i x_i^2 = \left(\frac{1}{2}\right)\left(I_y + I_z - I_x\right)$ for permutations of (*x, y, z*) = (*a, b, c*)). Although the relatively large non-zero P_{cc} planar moment is indicative of some out of plane motion within the complex, this value is nevertheless significantly smaller than P_{cc} for the structurally similar dimer, 1,1-DFE···FE (1.8805(7) u Å^2, [9]).

More detailed structural information may be obtained both *via* a least-squares fit of intermolecular structural parameters to experimental moments of inertia for the normal and four ^{13}C-containing isotopologues [23], and by application of Kraitchman's equations for single isotopic substitution [24, 25] to determine principal axis coordinates of the four substituted carbon atoms.

Table 5. Literature structure for FE [26]. Distances are in Å and angles in degrees. See Figure 2a for atom numbering.

Parameter	Value
$R(C_1–H_3)$	1.087
$R(C_1–H_4)$	1.077
$R(C_2–H_5)$	1.082
$R(C_2–F_6)$	1.347
$R(C_1=C_2)$	1.329
$\theta(H_3–C_1=C_2)$	120.9
$\theta(H_4–C_1=C_2)$	119.0
$\theta(H_5–C_2=C_1)$	129.2
$\theta(F_6–C_2=C_1)$	120.8

The least-squares fit was performed using the STRFIT program [23] and assuming monomer structures were unchanged within the dimer. Structural parameters for FE monomer are given in Table 5 [26]. A more recent and more precise monomer structure is also available [27]; however, we have continued to utilize parameters from Reference [26] for more consistent comparison with structures of previous FE-containing dimers. The resulting difference in intermolecular parameters is expected to be small. With the assumption of a planar dimer structure, three parameters are needed to uniquely define the relative orientation of the two FE molecules. In the present work, these were chosen as the F6···H9 distance (R) and two angles, C7-H9···F6 (θ) and H9···F6-C2 (ϕ), Figure 2(a). Since for a planar structure $I_a + I_b = I_c$, each isotopologue provides only two independent structural parameters; thus, pairs of moments of inertia from each isotopologue were utilized for the least-squares fit, giving a series of trials, each of which fitted three structural parameters to ten moments of inertia (Table 6). The best structure fits (based on lowest root-mean-square (RMS) deviations of observed minus calculated moments of inertia) were those that included I_a; however, uncertainty in the A rotational constant is large because the majority of assigned transitions are *a*-type. To try to mitigate the increased uncertainties arising from utilizing A for structure determination, a second fit was performed in which structural parameters were fitted to P_{aa} and P_{bb} planar moments. The standard deviation of this fit is larger than for the result obtained from fitting moments of inertia, although the structural results are similar. For this reason, we feel that the inertial fit of I_a and I_c from the normal and each isotopologue to the three structural parameters of the dimer is the most reliable fit, and this is reported in Table 6 ("Best" column).

Kisiel's KRA and EVAL programs [25] were used to extract coordinates of all four carbon atoms within the dimer principal axis system (Table 7, r_s coordinates), allowing the

relative alignment of the two double bonds to be determined. Structural parameters derived from this approach are also reported in Table 6 for comparison with inertial fit results. C=C bond lengths from the Kraitchman analysis can be used to gauge the accuracy of the r_s coordinates and resulting structural parameters. Unfortunately, the small *b*-coordinates of three of the four carbon atoms contribute to high uncertainties in the r_s parameters, giving C=C bond lengths of 1.305(7) Å and 1.368(13) Å, compared to a literature value of 1.329(6) Å [26]. As a result of these high uncertainties, while the r_s results provide confirmation of the general structural arrangement of the FE molecules, quantitative analysis of r_s results is not as useful.

D. Dipole moment

A total of 27 Stark shift measurements were made on 6 separate *M* components from 3 different rotational transitions, at fields of up to ~230 V cm^{-1}. Kisiel's QSTARK [28] program was used to fit μ_a and μ_b to the Stark shifted transition frequencies, with rotational and distortion constants fixed to the values obtained from SPFIT (Table 1). Because QSTARK utilizes a Watson *A*-reduction Hamiltonian, the fitted *S*-reduction constants were first converted to *A*-reduction values using Kisiel's CONVC routine [29]. The resulting dipole moment components are μ_a = 0.683(3) D, μ_b = 0.301(5) D, μ_{tot} = 0.746(5) D, consistent with MP2 calculations for *ab initio* Structure 3 (Table 4), while DFT calculations somewhat overestimate the total dipole (Table 3). Efforts to fit μ_c were unsuccessful, consistent with the planar nature of the dimer, and in contrast to the MP2/6-311++G(2d,2p) calculations. Full details of dipole fitting data are summarized in Supplementary Tables.

Table 6. Parameters resulting from least-squares fits of a distance and two angles (R, θ and ϕ) to pairs of moments of inertia or planar moments from the normal and four ^{13}C isotopologues of $(FE)_2$. The preferred structure is labeled "Best". Derived structural parameters from the r_s coordinates reported in Table 7 are also included for comparison. See Figure 2 for atom numbering.

	I_a, I_c (Best)	I_a, I_b	I_b, I_c	r_s
$R_{F6\cdots H9}$ / Å [a]	2.470(10)	2.481(10)	2.466(19)	
$\theta_{F6\cdots H9\text{-}C7}$ / ° [a]	157.9(4)	158.0(4)	155.6(7)	
$\phi_{H9\cdots F6\text{-}C2}$ / ° [a]	111.25(18)	111.22(17)	115.2(3)	
ΔI_{rms} / u Å^2 [b]	0.026	0.028	0.073	
H5⋯F12 / Å	2.399(7)	2.412(7)	2.420(13)	
C2-H5⋯F12 / °	153.5(3)	153.5(3)	149.2(5)	
H5⋯F12-C8 / °	125.6(3)	125.6(2)	128.4(5)	
C1-C2⋯C7 / °	177.50(12)	177.53(11)	174.80(24)	176.3(1.4)
C1-C2⋯C8 / °	164.07(13)	164.09(12)	166.88(25)	164.8(1.4)
C2⋯C7-C8 / °	86.8(3)	86.9(3)	85.7(6)	85.7(4)
C2⋯C8-C7 / °	74.8(3)	74.7(3)	76.0(6)	75.4(3)
C2⋯C7 / Å	4.055(8)	4.067(7)	4.102(15)	4.083(9)
C2⋯C8 / Å	4.1960(10)	4.2088(10)	4.2155(21)	4.2060(11)
C1⋯C2 / Å	1.329 [c]			1.305(7)
C7⋯C8 / Å	1.329			1.368(13)
R_{cm} / Å	3.9894(2)	4.0020(2)	3.9890(4)	

[a] Parameters varied during the least-squares fitting routine. Other displayed parameters are derived from the fitted structure – see text.
[b] Root-mean-square of $I_{observed} - I_{calculated}$ values for moments of inertia included in the least-squares fit.
[c] C=C distances within FE monomers from Ref. [26].

Table 7. Principal axis coordinates (in Å) of carbon atoms determined by use of Kraitchman's equations (r_s structure), and corresponding values for the preferred inertial fit structure (r_0 – see "Best" column of Table 6).

	$\|a\|$ (r_s)	$\|b\|$ (r_s)	a (r_0)	b (r_0)
C1	3.0025(5)	0.6182(70)	–2.9997(19)	0.6345(12)
C2	1.7490(9)	0.2563(239)	–1.7299(10)	0.2423(18)
C7	2.0916(7)	1.1279(78)	2.0889(82)	–1.1228(18)
C8	2.4565(6)	0.1902(109)	2.46510(7)	0.1518(43)

IV. Discussion

The planar T-like structure of the observed fluoroethylene dimer is analogous to the structure recently observed for FE···1,1-DFE [9], and comparison of the two structures may provide some insight into the variation of intermolecular interactions upon substitution of one hydrogen atom by a fluorine atom in unsaturated molecules. Each monomer acts as both a donor and an acceptor for a weak CH···F interaction. The H9···F6 contact (Figure 2) is nearly identical in the two species, with values of 2.470(10) Å in $(FE)_2$ and 2.463(16) Å in FE···1,1-DFE [9]. These distances both fall within the sum of van der Waals radii of H and F (1.20 + 1.47 = 2.67 Å [30]); thus, the H···F interactions are likely quite strong. The H5···F12 contact is 0.1 Å shorter in $(FE)_2$ (2.399(7) Å) than in FE···1,1-DFE (2.496(9) Å [9]), indicating a weaker interaction in the latter species, possibly as a result of the second fluorine atom in DFE drawing electron density away from the C–F bond that is participating in the intermolecular contact.

Intermolecular bond energies, E_B, may be estimated using a pseudodiatomic approximation based on a Lennard-Jones potential, according to equations (1) and (2) [31, 32], where k_s is the force constant for the intermolecular bond, μ is the pseudodiatomic reduced mass,

R_{cm} is the distance between the centers of mass of the two monomers, h is Planck's constant, D_J is the Watson S-reduction distortion constant, and all values are used in base SI units.

$$k_s = \frac{16\pi^4 (\mu R_{cm})^2[4B^4+4C^4-(B-C)^2(B+C)^2]}{hD_J} \quad (1)$$

$$E_B = \frac{1}{72} k_s R_{cm}^2 \quad (2)$$

This gives k_s = 5.0(3) N m^{-1}, E_B = 6.7(4) kJ mol^{-1} and ν = 61(2) cm^{-1} (with $\nu = (2\pi)^{-1}(k_s/\mu)^{½}$), confirming, as supposed above, that the $(FE)_2$ interaction energy is larger than was observed for the structurally similar FE···1,1-DFE, for which k_s = 3.19(4) N m^{-1} and E_B = 5.32(15) kJ mol^{-1}. Perhaps a more rigorous theoretical investigation of the electrostatic properties of these dimers, which is beyond the scope of the present work, would shed further light on the similarities and differences in the nature of the CH···F interactions in these species. As a simple first step, the MP2/aug-cc-pVDZ interaction energy ($E_{(FE)2} - 2E_{FE}$, using ZPE corrected energies and not accounting for basis set superposition error) is 10.2 kJ mol^{-1}, showing only order of magnitude agreement with the experimental estimate. Without more extensive computational studies, it will not be clear whether this discrepancy arises from assumptions inherent in the experimental estimate or flaws in the computational approach.

V. Conclusions

In the present work, a polar form of fluoroethylene dimer has been identified using chirped-pulse Fourier-transform microwave spectroscopy. Despite being predicted to lie ~57 cm^{-1} higher in energy than the more stable nonpolar isomer of the dimer at the ZPE corrected MP2/aug-cc-pVDZ level, and having relatively small dipole moment components, the significant

intensity of the present species in the rotational spectrum indicates that it is relatively abundant within the molecular expansion.

MP2/6-311++G(2d,2p) calculations presented significant difficulties when attempting to optimize expected planar dimer arrangements, and this is consistent with known weaknesses of Pople basis sets, as described in Reference 22. While resulting in optimized structures with similar energies, dipole moment components, and rotational constants, the Dunning aug-cc-pVDZ calculations largely avoided the difficulties with planar structures that the equivalently sized Pople basis set encountered. Less expensive optimizations at the ωB97X-D/6-31+G(d,p) level gave structurally similar stationary points, but the energy ordering and dipole moment components deviated significantly from the MP2 results. It is also clear from the number of remaining transitions visible in the broadband rotational spectrum that there is significant formation of larger FE clusters, and spectra have already been assigned for two species, believed to be $(FE)_3$ and $(FE)_4$, as well as for FE···Ne. A significant number of additional unassigned lines still remain within the 1 million FID broadband scan, and present work is focused on implementing more sophisticated analysis techniques (based on intensity variation as experimental parameters are systematically varied) to identify groups of transitions belonging to related spectra. In addition to methods derived from a principal component analysis-like approach [5, 8], the extended cross correlation technique described by Jacobson [33] is presently being implemented as a complementary method for approaching large spectroscopic data sets [34].

Acknowledgements

The authors dedicate this paper to the memory of Dr. Jon Hougen and express our gratitude for his constant enthusiasm, encouragement and advice, particularly for the younger generation of spectroscopists, over the course of many years.

This work was supported by National Science Foundation grants NSF RUI-1664900 (EIU) and CHE-1531913 (UVa). The authors also acknowledge the assistance of Ms. Prashansa Kannangara for help with data collection on the resonant cavity FTMW instrument. Finally, we are grateful to one of the referees for bringing Reference 22 to our attention, prompting significant expansion of the computational work included in this manuscript.

Graphical Abstract

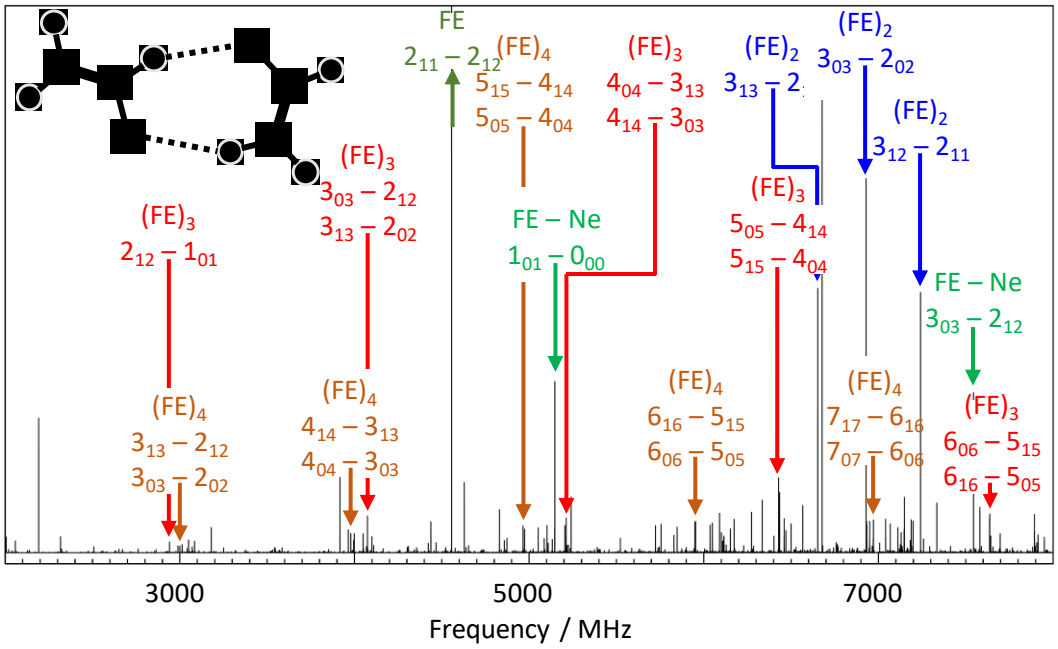

References

[1] M. Hyashi, T. Inagusa, Microwave Spectrum, Structure, and Dipole Moment of Vinyl Fluoride, J. Mol. Spectrosc. 138 (1989) 135-140.

[2] G.G. Brown, B.C. Dian, K.O. Douglass, S.M. Geyer, S.T. Shipman, B.H. Pate, A broadband Fourier transform microwave spectrometer based on chirped pulse excitation, Rev. Sci. Instrum., 79 (2008) 053103.

[3] J.L. Neill, B.J. Harris, A.L. Steber, K.O. Douglass, D.F. Plusquellic, B.H. Pate, Segmented chirped-pulse Fourier transform submillimeter spectroscopy for broadband gas analysis, Opt. Express, 21 (2013) 19743-19749.

[4] K.N. Crabtree, M.-A. Martin-Drumel, G.G. Brown, S.A. Gaster, T.M. Hall, M.C. McCarthy, Microwave spectral taxonomy: A semi-automated combination of chirped-pulse and cavity Fourier-transform microwave spectroscopy, J. Chem. Phys., 144 (2016) 124201.

[5] (a) R.A. Peebles, P. Kannangara, S.A. Peebles, B. Pate, New Approaches to Decoding Rotational Spectra: Applications to Fluoroethylene Microsolvation by CO_2, 73rd International Symposium on Molecular Spectroscopy, Talk TH02, Urbana, IL, June 19, 2018.; (b) R.A. Peebles, S.A. Peebles, P. Kannangara, T. Ariyaratne, B. Pate, C. West, Using Concentration Dependence of Microwave Spectra of 2-Component Mixtures to Identify Single Component Clusters - Application to $(Fluoroethylene)_n$ and $(1,1\text{-}Difluoroethylene)_n$, 74th International Symposium on Molecular Spectroscopy, Talk TC03, Urbana, IL, June 18, 2019.

[6] P.B. Kannangara, C.T. West, S.A. Peebles, R.A. Peebles, Towards microsolvation of fluorocarbons by CO_2: Two isomers of fluoroethylene-$(CO_2)_2$ observed using chirped-pulse Fourier-transform microwave spectroscopy, Chem. Phys. Lett. 706 (2018) 538-542.

[7] P.B. Kannangara, M.A. Martinez, B.H. Pate, S.A. Peebles, R.A. Peebles, Rotational Spectra, Structure and Dipole moment of the Fluoroethylene-Ne van der Waals Complex, unpublished results (2018).

[8] P.B. Kannangara, MS Thesis, Eastern Illinois University (2019).

[9] R.E. Dorris, S.A. Peebles, R.A. Peebles, Rotational spectrum and structural analysis of CH⋯F interactions in the vinyl fluoride⋯1,1-difluoroethylene dimer, J. Mol. Spectrosc. 335 (2017) 74-79.

[10] C. Pérez, S. Lobsiger, N.A. Seifert, D.P. Zaleski, B. Temelso, G.C. Shields, Z. Kisiel, B.H. Pate, Broadband Fourier transform rotational spectroscopy for structure determination: The water heptamer, Chem. Phys. Lett., 2013 (571) 1-15.

[11] Z. Kisiel, L. Pszczolkowski, I.R. Medvedev, M. Winnewisser, F.C. De Lucia, E. Herbst, Rotational Spectrum of Trans-Trans Diethyl Ether in the Ground and Three Excited Vibrational States, J. Mol. Spectrosc. 2005 (233), 231-243.

[12] H.M. Pickett, The fitting and prediction of vibration-rotation spectra with spin interactions, J. Mol. Spectrosc. 1991 (148) 371-377.

[13] T.J. Balle, W.H. Flygare, Fabry-Perot Cavity Pulsed Fourier Transform Microwave Spectrometer with a Pulsed Nozzle Particle Source. Rev. Sci. Instrum. 1981 (52) 33-45.

[14] J.J. Newby, M.M. Serafin, R.A. Peebles, S.A. Peebles, Rotational Spectrum, Structure and Modeling of the OCS-CS_2 van der Waals Dimer. Phys. Chem. Chem. Phys. 2005 (7) 487-492.

[15] J.M.L.J. Reinartz, A. Dymanus, Molecular constants of OCS isotopes in the (0110) vibrational state measured by molecular-beam electric-resonance spectroscopy, Chem. Phys. Lett. 24 (1974) 346-351.

[16] Gaussian 09W, Revision E.01, M.J. Frisch, G.W. Trucks, H.B. Schlegel, G.E. Scuseria, M.A. Robb, J.R. Cheeseman, G. Scalmani, V. Barone, G.A. Petersson, H. Nakatsuji, X. Li, M. Caricato, A. Marenich, J. Bloino, B.G. Janesko, R. Gomperts, B. Mennucci, H.P. Hratchian, J.V. Ortiz, A.F. Izmaylov, J.L. Sonnenberg, D. Williams-Young, F. Ding, F. Lipparini, F. Egidi, J. Goings, B. Peng, A. Petrone, T. Henderson, D. Ranasinghe, V.G. Zakrzewski, J. Gao, N. Rega, G. Zheng, W. Liang, M. Hada, M. Ehara, K. Toyota, R. Fukuda, J. Hasegawa, M. Ishida, T. Nakajima, Y. Honda, O. Kitao, H. Nakai, T. Vreven, K. Throssell, J.A. Montgomery, Jr., J.E. Peralta, F. Ogliaro, M. Bearpark, J.J. Heyd, E. Brothers, K.N. Kudin, V.N. Staroverov, T. Keith, R. Kobayashi, J. Normand, K. Raghavachari, A. Rendell, J. C. Burant, S.S. Iyengar, J. Tomasi, M. Cossi, J.M. Millam, M. Klene, C. Adamo, R. Cammi, J.W. Ochterski, R.L. Martin, K. Morokuma, O. Farkas, J.B. Foresman, D.J. Fox, Gaussian, Inc., Wallingford CT, 2013.

[17] Gaussian 09, Revision C.01, M. J. Frisch, G. W. Trucks, H. B. Schlegel, G. E. Scuseria, M. A. Robb, J. R. Cheeseman, G. Scalmani, V. Barone, B. Mennucci, G. A. Petersson, H. Nakatsuji, M. Caricato, X. Li, H. P. Hratchian, A. F. Izmaylov, J. Bloino, G. Zheng, J. L. Sonnenberg, M. Hada, M. Ehara, K. Toyota, R. Fukuda, J. Hasegawa, M. Ishida, T. Nakajima, Y. Honda, O. Kitao, H. Nakai, T. Vreven, J.A. Montgomery, Jr., J.E. Peralta, F. Ogliaro, M. Bearpark, JJ. Heyd, E. Brothers, K.N. Kudin, V.N. Staroverov, T. Keith, R. Kobayashi, J. Normand, K. Raghavachari, A. Rendell, J. C. Burant, S.S. Iyengar, J. Tomasi, M. Cossi, N. Rega, J.M. Millam, M. Klene, J.E. Knox, J.B. Cross, V. Bakken, C. Adamo, J. Jaramillo, R. Gomperts, R.E. Stratmann, O. Yazyev, A.J. Austin, R. Cammi, C. Pomelli, J.W. Ochterski, R.L. Martin, K. Morokuma, V.G. Zakrzewski, G.A. Voth, P. Salvador, J.J. Dannenberg, S. Dapprich, A.D. Daniels, O. Farkas, J.B. Foresman, J.V. Ortiz, J. Cioslowski, D.J. Fox, Gaussian, Inc., Wallingford CT, 2010.

[18] C.L. Christenholz, R.E. Dorris, R.A. Peebles, S.A. Peebles, Characterization of two isomers of the vinyl-fluoride···carbon dioxide dimer by rotational spectroscopy, J. Phys. Chem. A 2014 (118) 8765-8772.

[19] C.L. Christenholz, D.A. Obenchain, R.A. Peebles, S.A. Peebles, Rotational Spectroscopic Studies of C−H···F Interactions in the Vinyl Fluoride···Difluoromethane Complex, 2014 (118) 1610-1616.

[20] J. Zhang, M. Dolg, ABCluster: The Artificial Bee Colony Algorithm for Cluster Global Optimization, Phys. Chem. Chem. Phys. 2015 (17) 24173-24181.

[21] J. Zhang, M. Dolg, Global Optimization of Rigid Molecular Clusters by the Artificial Bee Colony Algorithm, Phys. Chem. Chem. Phys. 2016 (18) 3003-3010.

[22] D. Moran, A.C. Simmonett, F.E. Leach III, W.D. Allen, P.v.R. Schleyer, H.F. Schaefer III, The Popular Theoretical Methods Predict Benzene and Arenes to be Nonplanar, J. Am. Chem. Soc. 2006 (128) 9342-9343.

[23] Z. Kisiel, Least-squares mass-dependence molecular structures for selected weakly bound intermolecular clusters, J. Mol. Spectrosc. 2003 (218) 58-67.

[24] J. Kraitchman, Determination of Molecular Structure from Microwave Spectroscopic Data, Am. J. Phys. 1953 (21) 17-24.

[25] Kraitchman coordinates and structures from KRA and EVAL code, Z. Kisiel, PROSPE−Programs for Rotational Spectroscopy, http://www.ifpan.edu.pl/~kisiel/prospe.htm (accessed December 2019).

[26] D.R. Lide Jr., D. Christensen, An improved structure determination for vinyl fluoride, Spectrochim. Acta 1961 (17) 665-668.

[27] M. Hayashi, T. Inagusa, Microwave spectrum, structure and dipole moment of vinyl fluoride, J. Mol. Spectrosc. 1989 (138) 135-140.

[28] Z. Kisiel, J. Kosarzewski, B.A. Pietrewicz, L. Pszczolkowski, Chem. Phys. Lett. 2000 (325) 523-530.

[29] Z. Kisiel, PROSPE, Programs for Rotational Spectroscopy, http://www.ifpan.edu.pl/~kisiel/prospe.htm, accessed 3/5/2020; described in Z. Kisiel, in: J. Demaison et al. (Eds.), Spectroscopy from Space, Kluwer Academic Publishers, Dordrecht, 2001, 91-106.

[30] A. Bondi, van der Waals Volumes and Radii, J. Phys. Chem. 1964 (68) 441-451.

[31] D.J. Millen, Determination of stretching force constants of weakly bound dimers from centrifugal distortion constants, Can. J. Chem. 1985 (63) 1477-1479.

[32] T.J. Balle, E.J. Campbell, M.R. Keenan, W.H. Flygare, A new method for observing the rotational spectra of weak molecular complexes: KrHCl, J. Chem. Phys. 1980 (72) 922-932.

[33] M.P. Jacobson, S.M. Coy, R.W. Field, Extended Cross Correlation: A Technique for Spectroscopic Pattern Recognition, J. Chem. Phys. 1997 (107) 8349-8356.

[34] H.L. Fino, R.A. Peebles, S.A. Peebles, C.T. West, B.H. Pate, Implementing extended cross correlation as a tool to identify patterns in microwave spectra, and its application to

fluoroethylene/CO_2 clusters, American Chemical Society National Meeting, Philadelphia, PA, March 2020 (accepted abstract).